mater.scichina.com link.springer.com

Published online 1 January 2023 | https://doi.org/10.1007/s40843-022-2279-3
Sci China Mater 2023, 66(4): 1597–1606

Ultrafine cellulose nanocrystal-reinforced MXene biomimetic composites for multifunctional electromagnetic interference shielding

Na Wu[1†], Bin Li[2†], Fei Pan[3], Runa Zhang[2], Jiurong Liu[2*] and Zhihui Zeng[2*]

ABSTRACT **Polymers are widely employed to improve the mechanical properties of transition metal carbides and/or nitrides (MXenes) for constructing high-performance electromagnetic interference (EMI) shields. The challenges involve the insulating-polymer-induced compromise of electrical conductivity and EMI shielding performance of the MXene-based composites and the employment of nonrenewable, petrochemical polymers. Here, the one-dimensional, ultrafine, sustainable cellulose nanocrystals (CNCs) are efficiently employed to reinforce the MXene nanosheets, giving rise to high-strength, highly flexible biomimetic composites that maintain excellent electrical conductivity and EMI shielding effectiveness (SE). The freestanding MXene/CNC nanocomposites gain EMI SE values of 30 to 66 dB at thicknesses of approximately 2 to 14 μm, leading to ultrahigh specific SE and surface-specific SE values of 15,155 dB mm^{-1} and 54,125 dB cm^2 g^{-1}, respectively, which are comparable to those of the best EMI shields ever reported. Moreover, the excellent photothermal performance of the composite films was achieved, extending the application scenarios. Combined with the universal, facile, energy-efficient, and scalable ambient pressure drying preparation approach, the ultrathin, flexible, high-strength, and multifunctional CNC-reinforced MXene-based biomimetic films have shown great potential for applications in next-generation advanced flexible electronic or aerospace systems.**

Keywords: MXene, cellulose nanocrystal, EMI shielding, nanocomposite, multifunctional

INTRODUCTION

High-performance electromagnetic interference (EMI) shields with high EMI shielding effectiveness (SE), low thickness and density, high mechanical strength and flexibility, as well as considerable multifunctionalities, have attracted considerable attention for next-generation electronics with the capability of achieving electromagnetic compatibility or protection [1–6]. Because of their high electrical conductivity, good mechanical properties, large-aspect-ratio, and large specific surface area, low-dimensional carbon nanomaterials such as carbon nanotubes (CNTs) [7–11] and graphene [12–14], have shown great potential for use in constructing multifunctional, high-performance EMI shields. In particular, the combination of low-dimensional nanomaterials and polymers contributes to the preparation of electrically conductive nanocomposites with low density and cost, good mechanical performance, excellent chemical stability, and easy processability [3,8,15–17]. Both the formed nanomaterial-based conductive paths and the interfaces between nanomaterial and polymer can lead to the high loss capability of the incident electromagnetic wave (EMW), thus improving the EMI shielding performance of nanocomposites [18–24]. For instance, the CNTs were dispersed in polyurethane, epoxy, or polystyrene to form flexible composites with high EMI SE values at a low thickness [7,21,25]. Reduced graphene oxide was also combined with polyurethane to obtain flexible nanocomposites with an EMI SE of 31 dB at a thickness of 2 mm [26]. Despite the impressive progress, challenges in dispersing or processing the intrinsically inert carbon nanomaterials for constructing the macrostructures still exist, limiting the scalable preparation of the nanocarbon-based EMI shields. Moreover, the relatively low electrical conductivity of the carbon components hinders the achievement of high EMI SE of composites. Furthermore, most polymers are petrochemical and nonrenewable, which limits the application potentials of the polymeric EMI shields [21,25,27–31]. Developing sustainable, highly conductive, and robust nanocomposites for multifunctional, high-performance EMI shields in a cost-efficient, facile, and scalable preparation approach remains highly desired yet challenging.

In recent years, a novel type of two-dimensional (2D) transition metal carbide and/or nitride (MXene) sheets, commonly known as $Ti_3C_2T_x$ MXenes, have attracted increasing attention because of their large specific surface area, metallic conductivity, excellent mechanical properties, and processability in aqueous solution derived from surface hydrophilic functional groups (i.e., –O, –F, and –OH) [32–34]. These characteristics ensure that MXenes are suitable for use in fabricating high-performance EMI shields [33,35–37]. For example, MXene films were prepared by the vacuum filtration method and showed an excellent EMI SE of 68 dB at a thickness of approximately 11 μm [32], which led to an ultrahigh surface-specific SE (SSE/*d*, defined as the SE divided by the density and thickness of the shields, [7,32,38]) of 25,863 dB cm^2 g^{-1}. In comparison to the solid

[1] Department of Chemistry and Applied Biosciences, ETH Zurich, CH-8093 Zurich, Switzerland
[2] Key Laboratory for Liquid-Solid Structural Evolution and Processing of Materials, Ministry of Education and School of Materials Science and Engineering, Shandong University, Jinan 250061, China
[3] Department of Chemistry, University of Basel, Mattenstrasse 24a, BPR 1096, Basel, Switzerland
[†] These authors contributed equally to this work.
[*] Corresponding authors (emails: zhihui.zeng@sdu.edu.cn (Zeng Z); jrliu@sdu.edu.cn (Liu J))

copper or stainless steel with SSE values of about 30 dB cm^2 g^{-1} [39], MXenes are promising materials for use in lightweight, flexible, and high-performance EMI shields. However, the main challenges in constructing high-performance MXene-based shields mainly involve the weak gelation capability or interfacial interactions of MXene nanosheets, resulting in poor mechanical properties of the macrostructures [40–43]. Currently, the employment of polymers as matrixes or binders is the most common approach to reinforce the MXene-based EMI shields [28–30,32,44–47]. In particular, water-soluble polymers with hydrophilic groups could induce the generation of strong hydrogen bonding interactions with MXene nanosheets [29,32,44–47], promoting the dispersion of MXene nanosheets and improving the mechanical strength of the composites. For instance, aramid nanofiber [29,46], polyvinyl alcohol (PVA) [29,44], and sodium alginate [32] were employed to enhance the mechanical strength and modulus as well as the toughness of MXene-based films, showing high EMI SE values of 40, 28, and 57 dB at thicknesses of approximately 3, 100, and 9 μm, respectively. However, relatively large insulating gaps between MXene nanosheets are inevitable because of the introduced polymer chains, which significantly decreases the electrical conductivity and EMI SE of MXene-based composites. Biomass nanocellulose including cellulose nanofibers (CNFs) or nanocrystals (CNCs) [2,48–50], extracted from the most abundant polymer on earth, could have diameters of several to hundreds of nanometers. The ultrafine 1D fibrous structure of nanocellulose could decrease the insulating gaps between MXene nanosheets, thus maintaining the high electrical conductivity of MXene-based composites [2,51,52]. Although numerous CNF-reinforced MXene-based shields with high EMI shielding performance have been prepared [50,52–56], the exploration of CNC-enhanced MXene-based EMI shielding composites has rarely been reported. Similar to the CNF, CNC could act as sustainable nanoscale binders of MXene nanosheets because of its good gelation capability, excellent mechanical strength and modulus, and large aspect ratios [2,57,58]. Moreover, compared with CNF with a stronger tendency to agglomerate, which leads to the difficulty in obtaining CNF with small diameters, CNC with a lower density is easier to obtain. This helps reduce the insulating gaps between MXene sheets, thus improving the conductivity and EMI shielding performance of MXene-based composites. Notably, CNCs have become commercially available, which is beneficial to the scalable preparation of MXene-based EMI shields [58,59]. Therefore, accomplishing an energy-efficient and scalable preparation of high-performance CNC-enhanced MXene-based EMI shields is highly promising.

Here, we employed the ultrafine (a diameter of approximately 6 nm), large-aspect-ratio 1D CNC to reinforce MXene-based composites while maintaining high conductivity and EMI SE. Through a simple, facile, and scalable ambient-pressure drying approach, the flexible, robust, ultrathin, and highly conductive MXene/CNC composite films with excellent EMI SE were prepared. The nacre-like "brick and mortar" microstructure of the films was achieved because of the efficient intercalation of CNC between MXene nanosheets, leading to the significantly enhanced mechanical strength, modulus, and toughness of the MXene/CNC composites. The thicknesses and CNC contents of the composite films were controlled effortlessly, ensuring the wide-range controllability of the EMI SE values. The MXene/CNC composite films could reach EMI SE values of 30 to 65 dB at thicknesses of 2 to 14 μm. At an EMI SE of 30 dB that far surpasses the commercial SE value of 20 dB, an ultrahigh SSE value of 54,125 dB cm^2 g^{-1}, which is comparable to those of the best EMI shielding materials ever reported, was achieved for the MXene/CNC composite films. Combined with the efficient photothermal performance of the MXene/CNC composites, this work proposed a facile, cost-efficient, and scalable preparation approach for obtaining sustainable, robust, multifunctional, and high-performance MXene-based composites with great potential for applications in next-generation flexible electronic and aerospace systems.

EXPERIMENTAL SECTION

Preparation of the MXene aqueous dispersion and MXene/CNC composites

Aqueous Ti_3C_2 MXene dispersions were prepared by chemical etching of the aluminum layer and mechanical delamination of the Ti_3AlC_2 MAX [16,60]. Briefly, 2.0 g Ti_3AlC_2 MAX (Laizhou Kai Kai Ceramic Materials Co., Ltd, China) was added to 3.2 g lithium fluoride (Sigma-Aldrich, USA) dissolved in 40 mL hydrochloric acid (9 mol L^{-1}; Sigma-Aldrich, USA). Then, the dispersion was heated at a temperature of 35°C for 24 h for etching. Subsequently, the mixture was washed by centrifugation at 3500 r min^{-1} with ultrapure water to achieve a pH of approximately 6. Finally, after the suspension was vigorously shaken for 30 min and centrifuged at 3500 r min^{-1}, the supernatant MXene aqueous dispersion was collected with a concentration of 0.75 wt%. Then, the CNC aqueous dispersion with a similar concentration of 0.75 wt% was added and mixed with the MXene dispersion. After the mixed dispersion was cast in a polypropylene mold and dried at a temperature of 50°C, the ambient-pressure-dried freestanding MXene/CNC composite films with various CNC mass ratios were prepared. The thicknesses of the MXene/CNC composites were controlled by adjusting the mass ratio of the precursor mixed dispersion. In the same preparation process, the pure MXene films were also prepared.

Characterization

The microstructure was characterized by scanning electron microscopy (SEM; FEI Nano SEM 230), transmission electron microscopy (TEM; JEOL JEM2200fS), and atomic force microscopy (AFM; Bruker ICON3). The tensile stress-strain curves were obtained by a mechanical tester (IS-200N), and more than three samples for each component of the films were tested. The resistance (R) of the films was measured by a Keithley 4200 electrometer using the four-probe method and employed to calculate the electrical conductivity (δ) *via* the equation $\delta = l/(R \times A)$, where A and l are the effective area and length, respectively. The EMI SE of the films was measured by a vector network analyzer (Agilent 8517A) using the waveguide method. At least three specimens were tested for each component. The S-parameters were recorded and applied to calculate the total SE (SE_T), shielding by reflection (SE_R), and shielding by absorption (SE_A) as shown in our previous studies [7,16]. A xenon lamp (MC-PF300-UV, Merry Change) was used as the light source to conduct the photothermal conversion experiment of the films. The surface temperature of the film was measured in real time by a digital thermometer (unit-t ut325). Infrared thermal images of the films were obtained by a thermal imager (fotric223).

RESULTS AND DISCUSSION

The schematic of the preparation of the CNC-reinforced MXene-based composite films in an ambient-pressure drying approach is shown in Fig. 1a–c. First, CNC is extracted from cellulose fibers, which are the dominant component making up approximately 50% of wood biomass (Fig. 1a). The TEM images exhibited an average diameter of approximately 6 nm and an aspect ratio of approximately 50 for the 1D CNCs; thus, the transparent, stable CNC aqueous dispersion with obvious Tyndall effect was shown (Fig. 1d). Then, the MXene aqueous dispersion with a high zeta potential of approximately −40 mV was prepared *via* the chemical etching and mechanical delamination of the MAX precursors with a compact rock-like structure (Fig. S1a). The preparation details of the MXene nanosheets have been presented in our previous studies [16,60]. According to the TEM and electron diffraction data, the MXene sheets have an average lateral size of approximately 2 μm and a hexagonal atomic structure (Fig. 1e, f). Fig. 1g shows the AFM image of a single-layer MXene at a thickness of approximately 1.5 nm. The similar hydrophilic surface functional groups of CNC and MXene promoted a stable dispersion of MXene/CNC (Fig. S1b) [11,16]. Furthermore, CNCs could adhere well to MXene flakes because of the strong hydrogen bonding interactions formed between functional groups. This resulted in the intercalation of CNC between the MXene flakes and the formation of a nacre-like "brick and mortar" microstructure of the MXene/CNC films in the ambient-pressure drying process (Fig. 1c) [16,52,61]. This helped improve the mechanical strength of the MXene/CNC films, which could be easily manufactured even at thicknesses of approximately a few micrometers. A typical MXene/CNC composite film containing 30 wt% CNC exhibited mechanical ultraflexibility, including bendability and rollability (Fig. 1h).

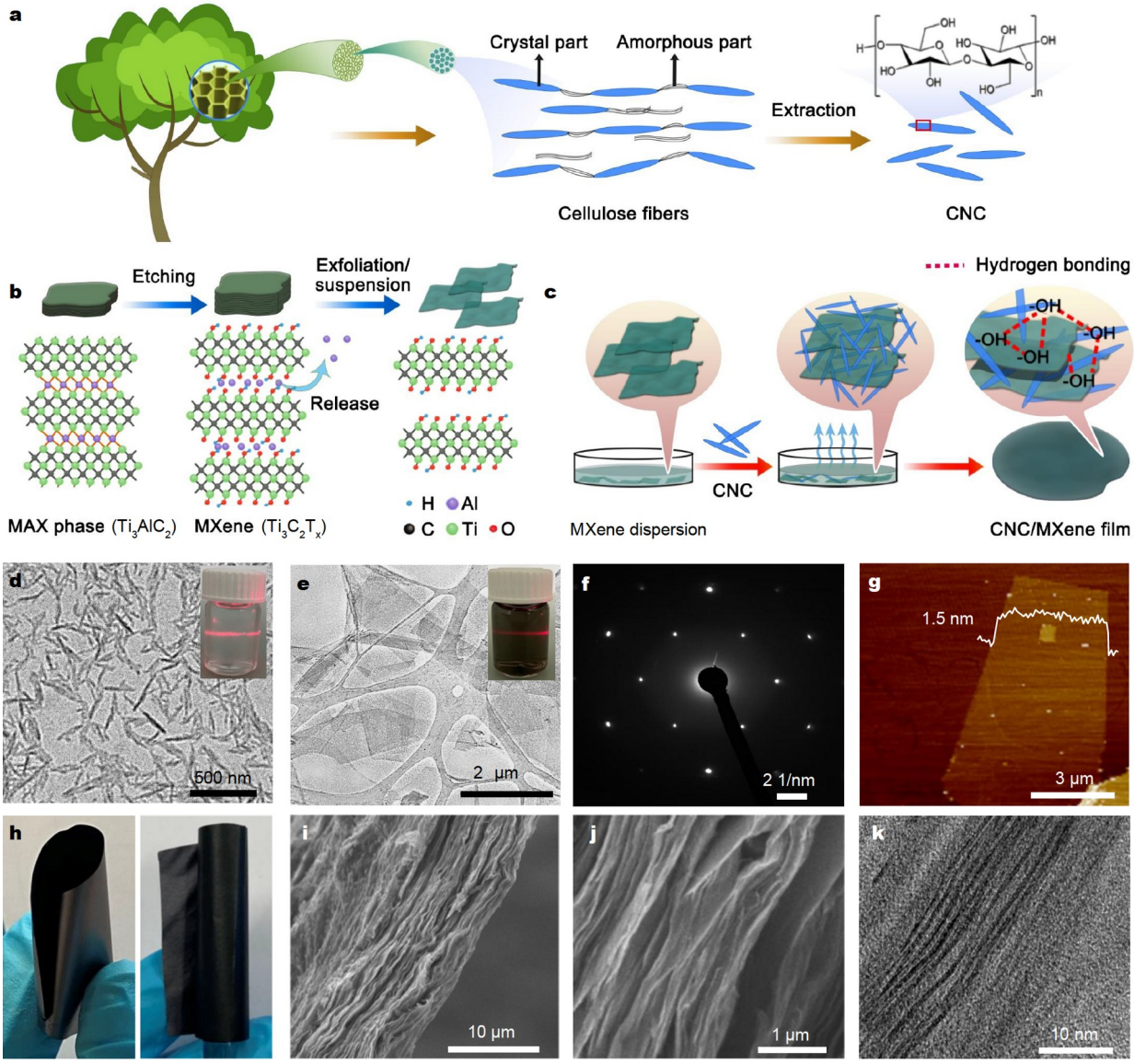

Figure 1 Manufacture and characterization of the MXene/CNC film. Schematics of the preparation of (a) CNC, (b) MXene, and (c) MXene/CNC composites. (d) TEM image of CNC. (e) TEM, (f) electron diffraction, and (g) AFM (inset shows the height profile of a monolayer) images of the MXene nanosheets. (h) Photographs of the freestanding MXene/CNC film showing ultraflexibility including bendability and rollability, (i, j) cross-sectional SEM and (k) TEM images of the MXene/CNC composite films showing the layered microstructure.

The excellent mechanical properties of the composite films also contributed to the preparation of the freestanding films even at thicknesses as low as several micrometers (Fig. 1i–k).

The introduction of the CNC to the MXene-based films efficiently improved the mechanical properties, including tensile strength, Young's modulus, and fracture strain (Fig. 2a). First, with the increase in the CNC contents, the mechanical strength, modulus, and toughness of the MXene/CNC composites increased significantly. For instance, the introduction of 50 wt% CNC to the MXene-based composites resulted in a significant enhancement in tensile strength, modulus, and mechanical toughness, which showed an increase of 590%, 300%, and 720%, respectively (Fig. 2b), in comparison with those of pure MXene films. Furthermore, excess CNCs led to decrease in mechanical strength and modulus because of decreased CNC-MXene interfaces, which were instrumental in promoting stress transfer in the composites. However, compared with those of pure MXene films, the intercalation of CNC, resulting in the biomimetic nacre-like microstructure of the MXene/CNC composites, still contributed to an obvious enhancement in the mechanical strength, modulus, and toughness, indicating the important role that CNCs play in achieving robust and durable composites.

Moreover, the employment of ultrafine 1D CNC helped retain the small insulating gaps between MXene sheets, which could maintain the high electrical conductivity of the composites. Because of the intercalation of CNCs, the (002) characteristic peak in the X-ray diffraction (XRD) patterns of the MXene-based films slightly downshifted with the increase in CNC contents, corresponding to a slightly increased interlayer spacing between MXene nanosheets of the composites (Fig. 2c). Compared with that of 1.24 nm for the pure MXene films, the MXene/CNC films with 30 and 70 wt% CNCs showed interlayer gaps of 1.27 and 1.31 nm, respectively. These small insulating gaps were instrumental in maintaining the high conductivity of the MXene/CNC composites [16,51]. By contrast, the commonly used polymers, such as PVA or polyethylene glycol (PEG), were used to prepare the MXene-based films with various polymer contents, which showed a more significantly decreased conductivity with increased polymer contents (Fig. 2d). For instance, at a polymer content of 30 wt%, the MXene/PVA and MXene/PEG composites showed conductivities of 3.0 and 7.3 S cm^{-1} respectively, which are three orders of magnitude lower than that of the MXene/CNC composites with 30 wt% CNC (Fig. 2d). The high conductivity maintained for the MXene/CNC composites derived from the efficient use of ultrafine 1D CNC between MXene layers was instrumental in achieving excellent EMI shielding performance. Briefly, in addition to the significantly enhanced mechanical performance, CNC could maintain the excellent electrical conductivity of the MXene-based films.

The X-band EMI shielding performance of the same mass of MXene-based films with various CNC contents was assessed (Fig. 3a). With the increase in CNC content, the EMI SE decreased. However, the high EMI SE values of the MXene/CNC composites could be maintained even with the increase in CNC mass ratios, e.g., for the same mass of MXene-based composite films, the EMI SE values of the pure MXene films (approximately 4.8 μm), MXene/CNC films with 30 wt% CNC

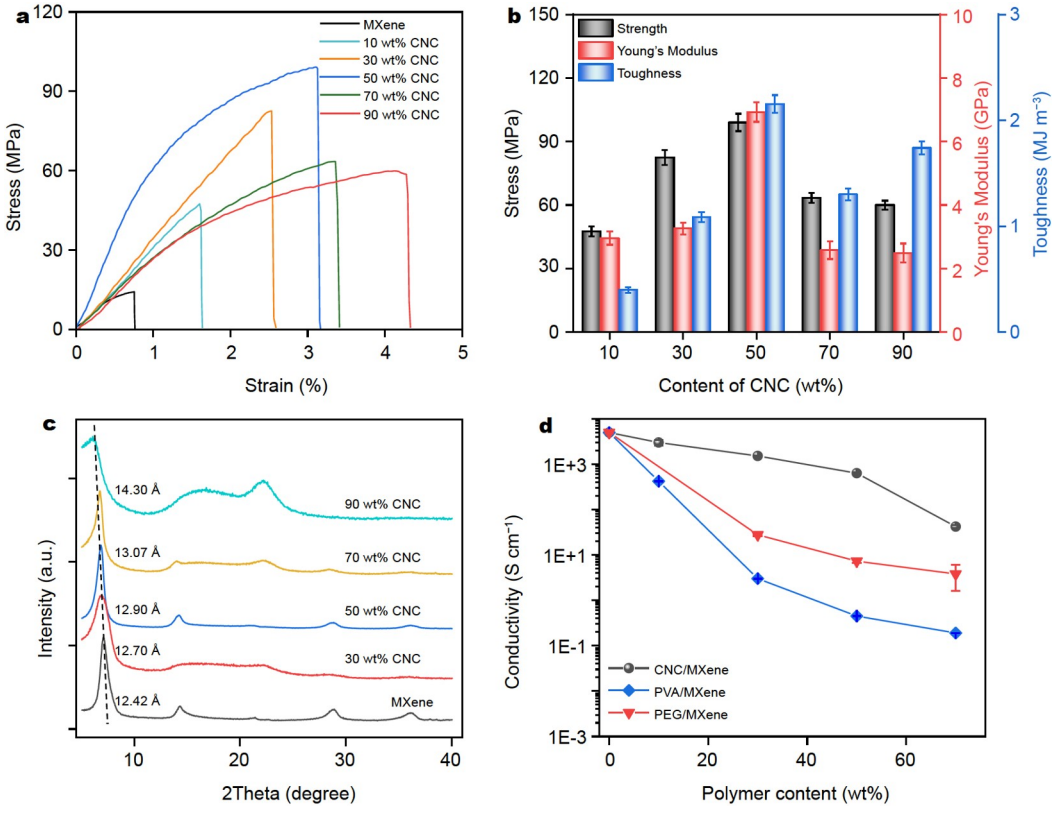

Figure 2 Properties and structure characterization of the MXene/CNC films. (a) Tensile stress-strain curves of the MXene-based composites with various CNC contents and (b) the corresponding tensile strength, modulus, and toughness. (c) XRD patterns of the MXene-based composites with various CNC contents. (d) Electrical conductivities of the MXene/CNC, MXene/PVA, and MXene/PEG composites with various mass ratios of polymers.

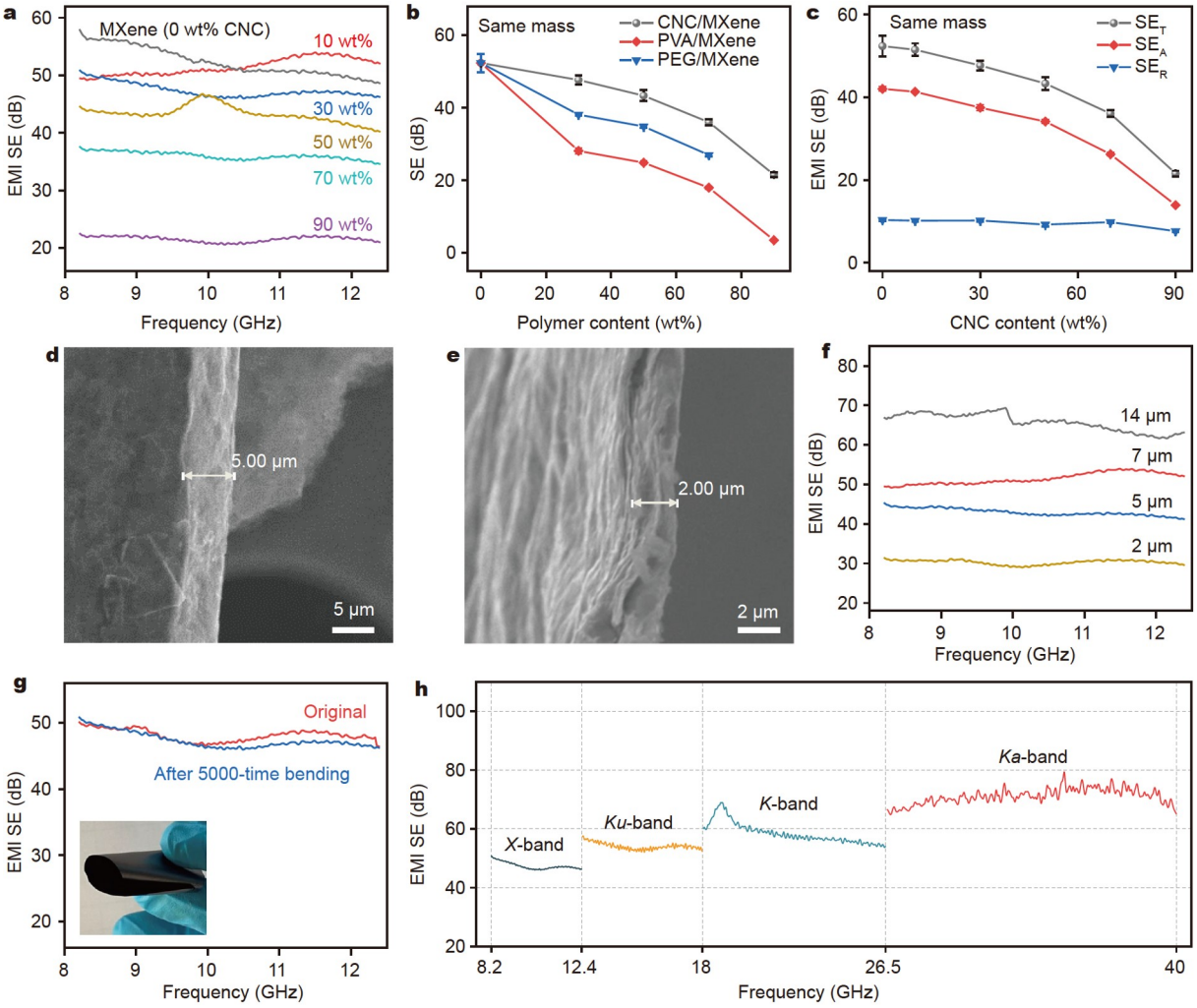

Figure 3 EMI shielding performance. (a) X-band EMI SE of the MXene/CNC films with various CNC contents, (b) EMI SE values for the MXene/CNC, MXene/PVA, and MXene/PEG composites with various mass ratios of polymers, and (c) EMI shielding performances (SE_T, SE_A, and SE_R) at 10 GHz of the MXene/CNC films with various CNC contents. SEM images of MXene/CNC composites with 30 wt% CNC films at thicknesses of approximately (d) 5 and (e) 2 μm. (f) X-band EMI SE of the MXene/CNC composites (30 wt% CNC) with various thicknesses. (g) X-band EMI SE of the MXene/CNC composites before and after being bent 5000 times at a bending speed of 0.5 Hz. (h) EMI SE of the MXene/CNC composites in the ultrabroadband GHz frequency range.

(approximately 7 μm), and MXene/CNC films with 50 wt% CNC were 52, 48, and 43 dB, respectively. Even at a CNC content of 90 wt%, the EMI SE values were higher than the commercial SE value of 20 dB, corresponding to a 99% attenuation of the incident EM waves [56,62,63]. To better understand the important influence of the introduced ultrafine 1D CNCs on the EMI shielding performance of the MXene-based films, the EMI SEs of the same mass of MXene/PEG, MXene/PVA, and MXene/CNC composite films were compared (Fig. 3b). Notably, the MXene/CNC composite films showed higher EMI SE values than the MXene/PEG and MXene/PVA composites at the same polymer mass ratios. For instance, at the polymer content of 30 wt%, the EMI SE values of the MXene/CNC, MXene/PEG, and MXene/PVA composite films reached 48, 38, and 28 dB, respectively. At the polymer content of 90 wt%, the MXene/PVA composite films even had too low EMI SE values to be used. In the previously reported studies [52,64], CNFs, with diameters of 20–50 nm, were used to reinforce the MXene-based films, which only showed an EMI SE of 25.8 dB at a thickness of 47 μm; thus, its performance is not as good as our MXene/CNC composites embedded with ultrafine CNCs. In summary, our ultrafine 1D CNCs exhibited superior properties beneficial to the preparation of robust MXene-based composites without significantly compromising the electrical conductivity and EMI SE, thereby outperforming other conductive polymer composites (CPCs) (Table S1).

The EMI shielding performance of the conductive composites was determined by the reflection, absorption, and multiple reflections of incident EMWs [7,17,38], which referred to the mobile charge carriers, electric dipoles, and interior interfaces/surfaces, respectively. Thus SE_T, SE_R, and SE_A were calculated (Fig. 3c). SE_R slightly decreased with the increase in CNC contents because of the slightly decreased electrical conductivity of the MXene/CNC composites. In addition to the abundant charge carriers originating from MXene and the generated electric dipoles derived from the MXene functional groups under the electric field of incident EMWs [57], the layered microstructure of the MXene nanosheets is beneficial to the multiple reflections or scatterings of incident EMWs. Combined with the interfacial polarization capability derived from the large mismatch of

conductivity in the interfacial region of MXene and CNC, the EMW absorbing capability of the MXene/CNC composites can be improved. SE_A decreased with the decrease in MXene content or increase in CNC content. However, SE_A was still higher than SE_R, which was similar to that of the other CPCs ever reported [25,31,34,65].

In the facile casting approach, the MXene/CNC composites' thicknesses were controlled easily, contributing to the wide-range controllability of the EMI SE values (Fig. 3d–f). The EMI SE values of 30 wt% MXene/CNC composites increased with the increase in thickness, e.g., the EMI SE reached 43 and 66 dB at thicknesses of 5 and 14 μm, respectively (Fig. 3d, f). Even at a thickness as low as 2.0 μm, the EMI SE value was more than 30 dB (Fig. 3e, f), with the transmission of EMWs being less than 0.001%. Moreover, the EMI shielding performance became stable for MXene/CNC composites upon mechanical deformation, e.g., the EMI SE changed slightly even when the composite films were bent for 5000 cycles (Fig. 3g). Furthermore, in the ultrabroadband GHz frequency range of 8.2 to 40 GHz, covering the X-band (8.2–12.4 GHz), Ku-band (12.4–18 GHz), K-band (18–26.5 GHz), and Ka-band (26.5–40 GHz), EMI SE values of more than 50 dB could be obtained for the thin MXene/CNC composite films (Fig. 3h), further showing their application potentials. Briefly, the controllable and high EMI SE in the ultrabroadband frequency range as well as the high EMI shielding stability, ensure that the MXene/CNC composites can be employed in high-performance EMI shielding architectures.

Notably, a high SE accompanied by a minimum thickness is vital to the development of high-performance EMI shielding architectures [2,3,7,32]. The high EMI SE of the MXene/CNC composites was maintained at such a low thickness. To make a comparison, SE/*d*, defined as the SE divided by the thickness, was employed as a critical index to evaluate the EMI shielding performance. The SE/*d* values reached 4700 to 15,155 dB mm^{-1} for the MXene/CNC films, significantly surpassing those of most previously reported shields (Table S1). Further considering the low density, the SSE/*d* value of the MXene/CNC composite films could reach 16,786 to 54,125 dB cm^2 g^{-1}, which are comparable to that of the best EMI shields (Fig. 4a). More details on the comparison of typical EMI shields are listed in Table S1. For example, even at a high EMI SE 66 dB, the MXene/CNC composite films exhibited an SSE/*d* value of 16,786 dB cm^2 g^{-1}, which was two to three orders of magnitude larger than that of the commonly employed EMI shields or CPCs. The excellent EMI shielding performance of the MXene/CNC composite was ascribed to the synergy of a highly conductive, MXene layer, ultrafine 1D CNCs intercalated between MXene nanosheets, and numerous interfaces generated between the MXene and CNCs, which synergistically led to the high conduction loss, strong polarization loss, and multiple reflections or scatterings of incident EMWs (Fig. 4b). Moreover, the nacre-like "brick and mortar" microstructure of the MXene/CNC composites and the strong interfacial interactions between MXene and CNCs were instrumental in achieving high mechanical strength and toughness. Regarding the EMI SE and tensile strength, the MXene/CNC composite films performed better than most macrostructures (Fig. 4c). In other words, the rational utilization of the ultrafine, 1D CNCs led to the excellent mechanical strength of the MXene/CNC composites without compromising the excellent EMI SE of MXene. Combined with the universal, cost-efficient, and scalable preparation method, the lightweight, flexible, ultrathin, and high-strength MXene/CNC composites

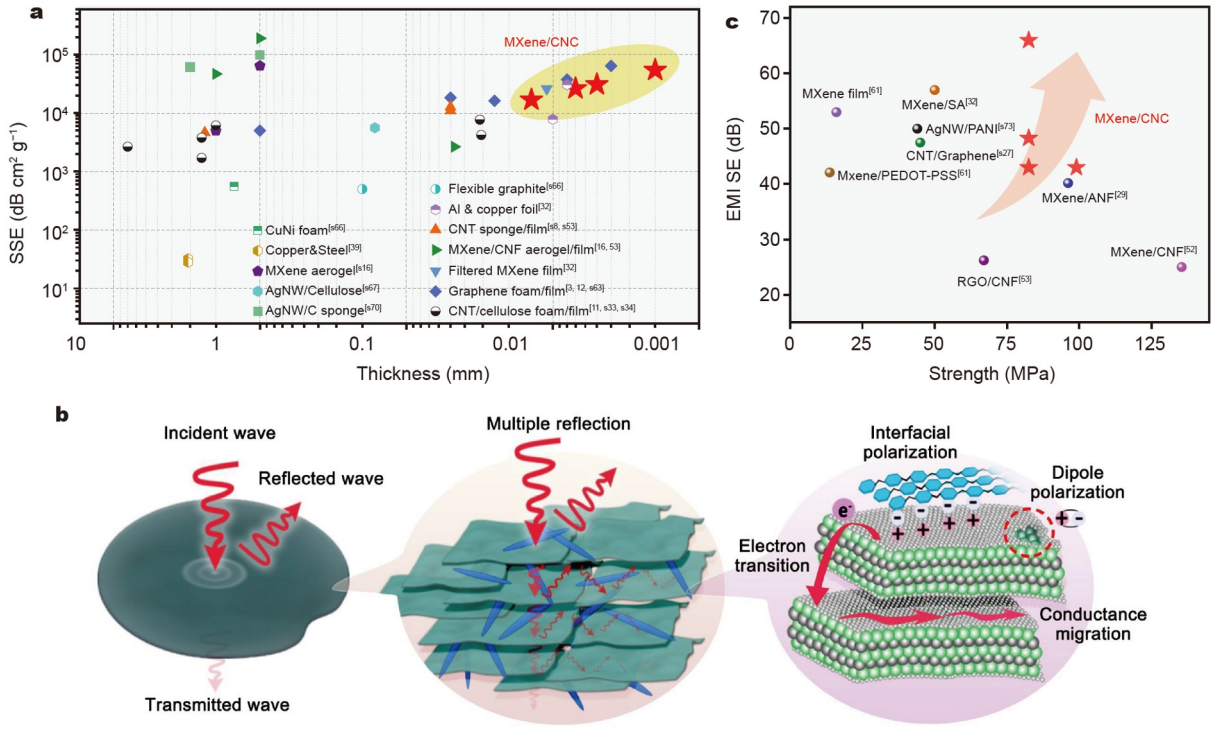

Figure 4 Performance comparison and EMI shielding mechanism. (a) Comparison of the SSE values of typical EMI shields with various thicknesses. (b) Schematic of the proposed EMI shielding mechanism of the MXene/CNC composite films with excellent EMI shielding performance. (c) Comparison of the MXene/CNC films with other shields in terms of EMI SE and tensile strength.

show excellent EMI shielding performance and application potentials in spacecraft, aircraft, or portable electronics.

The integration of other efficient functionalities into the EMI shields is important for next-generation electronics with the Internet of Things capability [66–68]. The local surface plasmon resonance effect and metal-like characteristics of MXene contributed to the excellent photothermal performance of the flexible MXene/CNC films [69]. Herein, the photothermal conversion performance of the MXene/CNC composite films was explored under the irradiation of a xenon lamp simulating sunlight. The surface temperature of the MXene/CNC films increased and reached the equilibrium temperature rapidly (Fig. 5a). A high equilibrium temperature of 80°C could be achieved for the films with an MXene content of only 10 wt% when the light power density was 150 mW cm^{-2}, which was superior to that of 52°C for the pure CNC film. The equilibrium temperatures of the MXene/CNC films containing 30, 50, 70, and 90 wt% MXene linearly increased to 82, 84, 88, and 92°C, respectively (Fig. 5b), which effectively proved the critical role that MXene played in improving the photothermal performance of the composite films. The equilibrium temperature was constant at a fixed light power density and could be easily adjusted by controlling the light power density. For example, the equilibrium temperatures of the films rapidly reached 37, 46, 67, 82, and 106°C at power densities of 25, 50, 100, 150, and 200 mW cm^{-2}, respectively (Fig. 5c). The infrared thermal images with uniform temperature distribution (Fig. 5d) further showed the stable and uniform heating performance of the films. As a typical instance, the flexible film was attached to human skin to demonstrate its potential as a photothermal therapy device. The film could be heated rapidly from room temperature to a suitable hyperthermia temperature of 56°C even at a low light power density (Fig. 5e). Furthermore, we tested the photothermal stability of the films at light power densities of 100 and 150 mW cm^{-2}. The temperature change could be regulated by turning the light on and off (Fig. 5f). Moreover, the stable temperature of the composite films could be maintained for a long period or after the films were employed many times (Fig. 5g). The film showed a rapid cooling process when the light was turned off, also demonstrating excellent photothermal stability and reliability, which is critical for the heaters in practical applications. Briefly, the MXene/CNC composite films exhibit great potential for fast, reversible, and reliable wearable heaters with outstanding photothermal performance.

CONCLUSIONS

We employed renewable CNCs to reinforce MXene-based films without significantly compromising the electrical conductivity

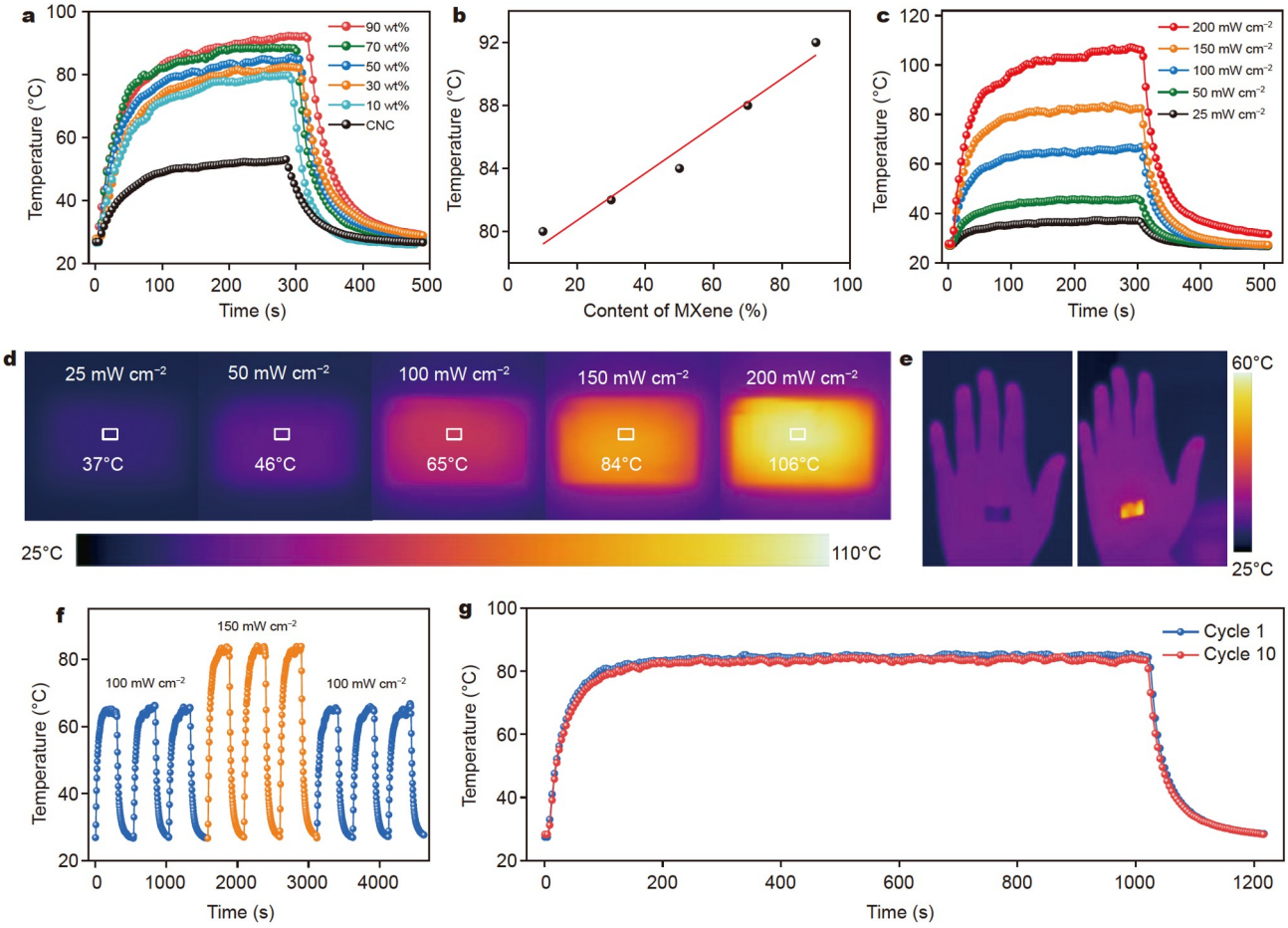

Figure 5 Photothermal performances of the MXene/CNC composite films. (a) Photothermal curves of the films with various MXene contents under xenon lamp irradiation at a power density of 150 mW cm^{-2}. (b) Equilibrium temperatures of the MXene/CNC composite films with various MXene contents. (c) Photothermal curves of the 50 wt% MXene films at various light power densities. The infrared thermal images of the films (d) at various light power densities and (e) used as wearable thermotherapy. (f) Photothermal curves of the 50 wt% MXene films under the on/off light cycles. (g) Lifetime and stability tests of the films after ten cycles.

and EMI shielding performance *via* a cost-efficient, facile, and scalable ambient-pressure drying preparation approach. Ultrafine, high-strength, low-density, and large-aspect-ratio 1D CNCs were efficiently intercalated between MXene nanosheets, resulting in freestanding biomimetic composite films with excellent mechanical strength, modulus, toughness, and ultraflexibility, high conductivity, and controllable and outstanding EMI shielding performance. The CNC-reinforced MXene-based films reached EMI SE values of 30 to 66 dB at thicknesses of 2 to 14 μm. Excellent SE/*d* and SSE values of up to 15,155 dB mm^{-1} and 54,125 dB cm^2 g^{-1}, respectively, were achieved for the MXene/CNC composites, far exceeding typical CPCs or most EMI shields ever reported. Compared with the other MXene/polymer nanocomposites including MXene/PVA or MXene/PEG films at similar polymer contents, our CNC-reinforced MXene-based composites performed better in both electrical conductivity and EMI SE. This was attributed to the synergy of the ultrafine 1D CNC and 2D highly conductive MXene, as well as the abundant MXene-CNC interfaces generated, enabling excellent conduction and polarization losses and EMI shielding performance. Combined with the integrated photothermal performance, this work demonstrates that sustainable, scalable, high-performance, and multifunctional MXene-based biomimetic composites have great potential for applications in next-generation flexible electronics or aerospace systems.

Received 2 August 2022; accepted 5 October 2022; published online 1 January 2023

1 Iqbal A, Shahzad F, Hantanasirisakul K, *et al.* Anomalous absorption of electromagnetic waves by 2D transition metal carbonitride Ti_3CNT_x (MXene). Science, 2020, 369: 446–450
2 De France K, Zeng Z, Wu T, *et al.* Functional materials from nanocellulose: Utilizing structure-property relationships in bottom-up fabrication. Adv Mater, 2020, 33: 2000657
3 Chen Z, Xu C, Ma C, *et al.* Lightweight and flexible graphene foam composites for high-performance electromagnetic interference shielding. Adv Mater, 2013, 25: 1296–1300
4 Zhou Z, Song Q, Huang B, *et al.* Facile fabrication of densely packed Ti_3C_2 MXene/nanocellulose composite films for enhancing electromagnetic interference shielding and electro-/photothermal performance. ACS Nano, 2021, 15: 12405–12417
5 Guan X, Yang Z, Zhou M, *et al.* 2D MXene nanomaterials: Synthesis, mechanism, and multifunctional applications in microwave absorption. Small Struct, 2022, 3: 2200102
6 Zhao Y, Ji G. Multi-spectrum bands compatibility: New trends in stealth materials research. Sci China Mater, 2022, 65: 2936–2941
7 Zeng Z, Jin H, Chen M, *et al.* Lightweight and anisotropic porous MWCNT/WPU composites for ultrahigh performance electromagnetic interference shielding. Adv Funct Mater, 2016, 26: 303–310
8 Song Q, Ye F, Yin X, *et al.* Carbon nanotube-multilayered graphene edge plane core-shell hybrid foams for ultrahigh-performance electromagnetic-interference shielding. Adv Mater, 2017, 29: 1701583
9 Zeng ZH, Wu N, Wei JJ, *et al.* Porous and ultra-flexible crosslinked mxene/polyimide composites for multifunctional electromagnetic interference shielding. Nano-Micro Lett, 2022, 14: 59
10 Al-Saleh MH, Sundararaj U. Electromagnetic interference shielding mechanisms of CNT/polymer composites. Carbon, 2009, 47: 1738–1746
11 Zeng Z, Wang C, Wu T, *et al.* Nanocellulose assisted preparation of ambient dried, large-scale and mechanically robust carbon nanotube foams for electromagnetic interference shielding. J Mater Chem A, 2020, 8: 17969–17979
12 Wei Q, Pei S, Qian X, *et al.* Superhigh electromagnetic interference shielding of ultrathin aligned pristine graphene nanosheets film. Adv Mater, 2020, 32: 1907411
13 Zhao S, Zhang HB, Luo JQ, *et al.* Highly electrically conductive three-dimensional $Ti_3C_2T_x$ MXene/reduced graphene oxide hybrid aerogels with excellent electromagnetic interference shielding performances. ACS Nano, 2018, 12: 11193–11202
14 Zhou T, Wu C, Wang Y, *et al.* Super-tough MXene-functionalized graphene sheets. Nat Commun, 2020, 11: 2077
15 Yousefi N, Sun X, Lin X, *et al.* Highly aligned graphene/polymer nanocomposites with excellent dielectric properties for high-performance electromagnetic interference shielding. Adv Mater, 2014, 26: 5480–5487
16 Zeng Z, Wang C, Siqueira G, *et al.* Nanocellulose-MXene biomimetic aerogels with orientation-tunable electromagnetic interference shielding performance. Adv Sci, 2020, 7: 2000979
17 Chung DDL. Electromagnetic interference shielding effectiveness of carbon materials. Carbon, 2001, 39: 279–285
18 Thomassin JM, Jérôme C, Pardoen T, *et al.* Polymer/carbon based composites as electromagnetic interference (EMI) shielding materials. Mater Sci Eng-R-Rep, 2013, 74: 211–232
19 Carey M, Barsoum MW. MXene polymer nanocomposites: A review. Mater Today Adv, 2021, 9: 100120
20 Regev O, ElKati PNB, Loos J, *et al.* Preparation of conductive nanotube-polymer composites using latex technology. Adv Mater, 2004, 16: 248–251
21 Li N, Huang Y, Du F, *et al.* Electromagnetic interference (EMI) shielding of single-walled carbon nanotube epoxy composites. Nano Lett, 2006, 6: 1141–1145
22 Zhang Y, Kong J, Gu J. New generation electromagnetic materials: Harvesting instead of dissipation solo. Sci Bull, 2022, 67: 1413–1415
23 Li B, Wang F, Wang K, *et al.* Metal sulfides based composites as promising efficient microwave absorption materials: A review. J Mater Sci Tech, 2022, 104: 244–268
24 Tian H, Qiao J, Yang Y, *et al.* ZIF-67-derived Co/C embedded boron carbonitride nanotubes for efficient electromagnetic wave absorption. Chem Eng J, 2022, 450: 138011
25 Arjmand M, Apperley T, Okoniewski M, *et al.* Comparative study of electromagnetic interference shielding properties of injection molded *versus* compression molded multi-walled carbon nanotube/polystyrene composites. Carbon, 2012, 50: 5126–5134
26 Hsiao ST, Ma CCM, Tien HW, *et al.* Using a non-covalent modification to prepare a high electromagnetic interference shielding performance graphene nanosheet/water-borne polyurethane composite. Carbon, 2013, 60: 57–66
27 Wang L, Qiu H, Song P, *et al.* 3D $Ti_3C_2T_x$ MXene/C hybrid foam/epoxy nanocomposites with superior electromagnetic interference shielding performances and robust mechanical properties. Compos Part A-Appl Sci Manufact, 2019, 123: 293–300
28 Rajavel K, Luo S, Wan Y, *et al.* 2D $Ti_3C_2T_x$ MXene/polyvinylidene fluoride (PVDF) nanocomposites for attenuation of electromagnetic radiation with excellent heat dissipation. Compos Part A-Appl Sci Manufact, 2020, 129: 105693
29 Weng C, Xing T, Jin H, *et al.* Mechanically robust ANF/MXene composite films with tunable electromagnetic interference shielding performance. Compos Part A-Appl Sci Manufact, 2020, 135: 105927
30 Wang L, Chen L, Song P, *et al.* Fabrication on the annealed $Ti_3C_2T_x$ MXene/epoxy nanocomposites for electromagnetic interference shielding application. Compos Part B-Eng, 2019, 171: 111–118
31 Al-Saleh MH, Saadeh WH, Sundararaj U. EMI shielding effectiveness of carbon based nanostructured polymeric materials: A comparative study. Carbon, 2013, 60: 146–156
32 Shahzad F, Alhabeb M, Hatter CB, *et al.* Electromagnetic interference shielding with 2D transition metal carbides (MXenes). Science, 2016, 353: 1137–1140
33 Han M, Shuck CE, Rakhmanov R, *et al.* Beyond $Ti_3C_2T_x$: MXenes for electromagnetic interference shielding. ACS Nano, 2020, 14: 5008–5016
34 Nepal D, Kennedy WJ, Pachter R, *et al.* Toward architected nanocomposites: MXenes and beyond. ACS Nano, 2021, 15: 21–28
35 Song P, Liu B, Qiu H, *et al.* MXenes for polymer matrix electromagnetic interference shielding composites: A review. Compos Commun, 2021, 24: 100653
36 Zhang Y, Ma Z, Ruan K, *et al.* Multifunctional $Ti_3C_2T_x$-(Fe_3O_4/polyimide) composite films with Janus structure for outstanding electro-

magnetic interference shielding and superior visual thermal management. Nano Res, 2022, 15: 5601–5609
37 Zhang Y, Ruan K, Gu J. Flexible sandwich-structured electromagnetic interference shielding nanocomposite films with excellent thermal conductivities. Small, 2021, 17: 2101951
38 Liu J, Zhang HB, Sun R, *et al.* Hydrophobic, flexible, and lightweight MXene foams for high-performance electromagnetic-interference shielding. Adv Mater, 2017, 29: 1702367
39 Shui X, Chung DDL. Nickel filament polymer-matrix composites with low surface impedance and high electromagnetic interference shielding effectiveness. J Elec Materi, 1997, 26: 928–934
40 Chen H, Wen Y, Qi Y, *et al.* Pristine titanium carbide MXene films with environmentally stable conductivity and superior mechanical strength. Adv Funct Mater, 2019, 30: 1906996
41 Zhao X, Vashisth A, Prehn E, *et al.* Antioxidants unlock shelf-stable $Ti_3C_2T_x$ (MXene) nanosheet dispersions. Matter, 2019, 1: 513–526
42 Wan YJ, Rajavel K, Li XM, *et al.* Electromagnetic interference shielding of $Ti_3C_2T_x$ MXene modified by ionic liquid for high chemical stability and excellent mechanical strength. Chem Eng J, 2021, 408: 127303
43 Zhang J, Kong N, Uzun S, *et al.* Scalable manufacturing of free-standing, strong $Ti_3C_2T_x$ MXene films with outstanding conductivity. Adv Mater, 2020, 32: 2001093
44 Xu H, Yin X, Li X, *et al.* Lightweight Ti_2CT_x MXene/poly(vinyl alcohol) composite foams for electromagnetic wave shielding with absorption-dominated feature. ACS Appl Mater Interfaces, 2019, 11: 10198–10207
45 Zhou Z, Liu J, Zhang X, *et al.* Ultrathin MXene/calcium alginate aerogel film for high-performance electromagnetic interference shielding. Adv Mater Interfaces, 2019, 6: 1802040
46 Xie F, Jia F, Zhuo L, *et al.* Ultrathin MXene/aramid nanofiber composite paper with excellent mechanical properties for efficient electromagnetic interference shielding. Nanoscale, 2019, 11: 23382–23391
47 Ling Z, Ren CE, Zhao MQ, *et al.* Flexible and conductive MXene films and nanocomposites with high capacitance. Proc Natl Acad Sci USA, 2014, 111: 16676–16681
48 Li T, Chen C, Brozena AH, *et al.* Developing fibrillated cellulose as a sustainable technological material. Nature, 2021, 590: 47–56
49 Wu T, Zeng Z, Siqueira G, *et al.* Dual-porous cellulose nanofibril aerogels *via* modular drying and cross-linking. Nanoscale, 2020, 12: 7383–7394
50 Zhan Z, Song Q, Zhou Z, *et al.* Ultrastrong and conductive MXene/cellulose nanofiber films enhanced by hierarchical nano-architecture and interfacial interaction for flexible electromagnetic interference shielding. J Mater Chem C, 2019, 7: 9820–9829
51 Tian W, VahidMohammadi A, Reid MS, *et al.* Multifunctional nanocomposites with high strength and capacitance using 2D MXene and 1D nanocellulose. Adv Mater, 2019, 31: 1902977
52 Cao WT, Chen FF, Zhu YJ, *et al.* Binary strengthening and toughening of MXene/cellulose nanofiber composite paper with nacre-inspired structure and superior electromagnetic interference shielding properties. ACS Nano, 2018, 12: 4583–4593
53 Yang W, Zhao Z, Wu K, *et al.* Ultrathin flexible reduced graphene oxide/cellulose nanofiber composite films with strongly anisotropic thermal conductivity and efficient electromagnetic interference shielding. J Mater Chem C, 2017, 5: 3748–3756
54 Cao W, Ma C, Tan S, *et al.* Ultrathin and flexible CNTs/MXene/cellulose nanofibrils composite paper for electromagnetic interference shielding. Nano-Micro Lett, 2019, 11: 72
55 Xin W, Xi GQ, Cao WT, *et al.* Lightweight and flexible MXene/CNF/silver composite membranes with a brick-like structure and high-performance electromagnetic-interference shielding. RSC Adv, 2019, 9: 29636–29644
56 Liu Q, Zhang Y, Liu Y, *et al.* Ultrathin, biomimetic multifunctional leaf-like silver nanowires/$Ti_3C_2T_x$ MXene/cellulose nanofibrils nanocomposite film for high-performance electromagnetic interference shielding and thermal management. J Alloys Compd, 2021, 860: 158151
57 Aeby X, Poulin A, Siqueira G, *et al.* Fully 3D printed and disposable paper supercapacitors. Adv Mater, 2021, 33: 2101328
58 Hausmann MK, Siqueira G, Libanori R, *et al.* Complex-shaped cellulose composites made by wet densification of 3D printed scaffolds. Adv Funct Mater, 2020, 30: 1904127
59 Hausmann MK, Rühs PA, Siqueira G, *et al.* Dynamics of cellulose nanocrystal alignment during 3D printing. ACS Nano, 2018, 12: 6926–6937
60 Zeng Z, Mavrona E, Sacré D, *et al.* Terahertz birefringent biomimetic aerogels based on cellulose nanofibers and conductive nanomaterials. ACS Nano, 2021, 15: 7451–7462
61 Liu R, Miao M, Li Y, *et al.* Ultrathin biomimetic polymeric $Ti_3C_2T_x$ MXene composite films for electromagnetic interference shielding. ACS Appl Mater Interfaces, 2018, 10: 44787–44795
62 Ma Z, Xiang X, Shao L, *et al.* Multifunctional wearable silver nanowire decorated leather nanocomposites for joule heating, electromagnetic interference shielding and piezoresistive sensing. Angew Chem Int Ed, 2022, 61: e202200705
63 Zhang Y, Gu J. A perspective for developing polymer-based electromagnetic interference shielding composites. Nano-Micro Lett, 2022, 14: 89
64 Cui Z, Gao C, Fan Z, *et al.* Lightweight MXene/cellulose nanofiber composite film for electromagnetic interference shielding. J Elec Materi, 2021, 50: 2101–2110
65 Yun T, Kim H, Iqbal A, *et al.* Electromagnetic shielding of monolayer MXene assemblies. Adv Mater, 2020, 32: 1906769
66 Chen X, Zhou M, Zhao Y, *et al.* Morphology control of eco-friendly chitosan-derived carbon aerogels for efficient microwave absorption at thin thickness and thermal stealth. Green Chem, 2022, 24: 5280–5290
67 Zhou M, Wang J, Wang G, *et al.* Lotus leaf-inspired and multifunctional Janus carbon Felt@Ag composites enabled by *in situ* asymmetric modification for electromagnetic protection and low-voltage joule heating. Compos Part B-Eng, 2022, 242: 110110
68 Yang Y, Wu N, Li B, *et al.* Biomimetic porous MXene sediment-based hydrogel for high-performance and multifunctional electromagnetic interference shielding. ACS Nano, 2022, 16: 15042–15052
69 Tan C, Dong Z, Li Y, *et al.* A high performance wearable strain sensor with advanced thermal management for motion monitoring. Nat Commun, 2020, 11: 3530

Acknowledgements This work was financially supported by the National Key R&D Program of China (2021YFB3502500), the Natural Science Foundation of Shandong Province (2022HYYQ-014), the Provincial Key Research and Development Program of Shandong (2019JZZY010312 and 2021ZLGX01), the "20 Clauses about Colleges and Universities (new)" (Independent Training of Innovation Team) Program of Jinan (2021GXRC036), the Joint Laboratory Project of Electromagnetic Structure Technology (637-2022-70-F-037), and Qilu Young Scholar Program of Shandong University (31370082163127). The authors acknowledge the assistance of Shandong University Testing and Manufacturing Center for Advanced Materials.

Author contributions Wu N designed the work and engineered the samples; Wu N and Li B performed the experiments; Wu N and Li B performed the data analysis; Wu N, Li B, and Pan F wrote the paper with support from Zeng Z and Liu J; Wu N, Li B, and Zhang R contributed to the theoretical analysis. All authors contributed to the general discussion.

Conflict of interest The authors declare that they have no conflict of interest.

Supplementary information Supplementary data are available in the online version of the paper.

Zhihui Zeng received his PhD degree in materials science and engineering from the National Center for Nanoscience and Technology (NCNST), University of Chinese Academy of Sciences, Beijing, China in 2016. Following his work as a postdoctoral research fellow at Nanyang Technological University, Singapore, and Swiss Federal Laboratories for Materials Science and Technology (Empa), Switzerland, he currently works at Shandong University, China. His research interests include the design, fabrication and application of polymer-based nanocomposites, nanostructured assemblies, and cellular materials.

Jiurong Liu obtained his PhD degee from Osaka University in 2004. Then, he worked as a postdoctoral fellow at the University of California at Los Angeles until 2008 before beginning his career as a full professor at the School of Materials Science and Engineering, Shandong University. His research interests include the synthesis of hybrid nanomaterials for energy storage and electromagnetic applications.

Na Wu obtained her PhD degree from the Department of Chemistry and Applied Biosciences, ETH Zurich, Switzerland, in 2021. Now, she works at ETH zurich as a postdoctoral fellow. Her research interests include the design and preparation of electromagnetic shielding materials.

Bin Li received his Bachelor's degree from Qingdao University of Technology in 2019. He is currently pursuing his PhD degree under the supervision of Professor Jiurong Liu at Shandong University. His research interests focus on the design, fabrication, and application of electromagnetic functional materials.

超细纤维素纳米晶增强MXene仿生复合材料的多功能电磁屏蔽性能

吴娜[1†], 李宾[2†], 潘飞[3], 张如娜[2], 刘久荣[2*], 曾志辉[2*]

摘要 聚合物用于改善过渡金属碳化物和/或氮化物(MXenes)的力学性能、构建高性能电磁(EMI)屏蔽结构面临以下挑战: 绝缘聚合物对MXene基复合材料导电性和电磁屏蔽性能的影响以及聚合物的不可再生性. 本文将一维、超细、可持续的纤维素纳米晶体(CNCs)用于增强MXene纳米片, 从而制备出高强度、高柔性、同时兼顾优异导电性和电磁屏蔽效能(SE)的仿生复合材料, 其性能优于目前报道的聚合物复合材料. 在厚度仅为2–14 μm的情况下, MXene/CNC纳米复合材料的电磁屏蔽效能分别达到30–66 dB, 比屏蔽效能和面比屏蔽效能分别达到15,155 dB mm^{-1}和54,125 dB $cm^2 g^{-1}$. 复合薄膜具有良好的光热性能, 扩展了其应用场景. 结合简便、高效、可规模化的常压干燥制备方法得到的超薄、柔韧、高强度、多功能的CNC增强MXene基仿生薄膜在下一代先进电子或航空航天领域显示出巨大的应用潜力.